INTERNATIONAL JOURNAL FOR NUMERICAL METHODS IN FLUIDS
Int. J. Numer. Meth. Fluids 2003; **41**:29–45 (DOI: 10.1002/fld.422)

Vorticity–velocity formulation of the 3D Navier–Stokes equations in cylindrical co-ordinates

Martin O. L. Hansen*,†, Jens Nørkær Sørensen and Wen Zhong Shen

Department of Mechanical Engineering, Fluid Mechanics Section, Building 403, Technical University of Denmark, 2800 Lyngby, Denmark

SUMMARY

A finite difference method is presented for solving the 3D Navier–Stokes equations in vorticity–velocity form. The method involves solving the vorticity transport equations in 'curl-form' along with a set of Cauchy–Riemann type equations for the velocity. The equations are formulated in cylindrical co-ordinates and discretized using a staggered grid arrangement. The discretized Cauchy–Riemann type equations are overdetermined and their solution is accomplished by employing a conjugate gradient method on the normal equations. The vorticity transport equations are solved in time using a semi-implicit Crank–Nicolson/Adams–Bashforth scheme combined with a second-order accurate spatial discretization scheme. Special emphasis is put on the treatment of the polar singularity. Numerical results of axisymmetric as well as non-axisymmetric flows in a pipe and in a closed cylinder are presented. Comparison with measurements are carried out for the axisymmetric flow cases. Copyright © 2003 John Wiley & Sons, Ltd.

KEY WORDS: vorticity–velocity formulation; Cauchy–Riemann equations; treatment of polar singularity in cylindrical co-ordinates

1. INTRODUCTION

Most incompressible Navier–Stokes algorithms are based on solving the equations in the primary pressure and velocity variables. In this formulation, it is necessary to solve the momentum equations for the velocity field along with a derived Poisson equation for the pressure. The role of the pressure is to ensure a solenoidal velocity field (continuity) and as the Poisson equation does not satisfy this *a priori*, some kind of coupling to the continuity equation is needed. Such coupling technique have been developed under names as SIMPLE, PISO and fractional step methods (e.g. References [1–4]). An alternative approach is to eliminate the pressure from the momentum equations by applying the curl operator on these, and introducing the vorticity as the curl of the velocity. This results in the vorticity–velocity formulation

* Correspondence to: M. O. L. Hansen, Department of Mechanical Engineering, Fluid Mechanics Section, Building 403, Technical University of Denmark, 2800 Lyngby, Denmark.
† E-mail: molh@mek.dtu.dk

Received 17 April 2002
Accepted 13 August 2002

of the Navier–Stokes equations, in which the momentum equations are replaced by vorticity transport equations

$$\frac{\partial \boldsymbol{\omega}}{\partial t} + \nabla \times (\boldsymbol{\omega} \times \mathbf{V}) = v \nabla^2 \boldsymbol{\omega} \tag{1}$$

where $\mathbf{V}$ and $\boldsymbol{\omega}$ denote the velocity and vorticity vector, respectively, and v is the kinematic viscosity. The pressure Poisson equation is replaced by a set of Cauchy–Riemann (C–R) type equations, consisting of the definition of vorticity (2), and the continuity equation (3), respectively.

$$\boldsymbol{\omega} = \nabla \times \mathbf{V} \tag{2}$$

$$\nabla \cdot \mathbf{V} = 0 \tag{3}$$

From its definition, the vorticity field has to satisfy the solenoidal constraint:

$$\nabla \cdot \boldsymbol{\omega} = 0 \tag{4}$$

Further, the following compatibility constraint must be satisfied, ensuring zero net mass flow across the boundary of the computational domain b:

$$\int \int_b \mathbf{V} \cdot \mathbf{n} \, \mathrm{d}A = 0 \tag{5}$$

where $\mathbf{n}$ denotes the unit normal vector on the boundary and $\mathrm{d}A$ is an infinitesimal surface area around the normal vector. By exploiting Equation (4), the vorticity transport equations can take different forms. Employing the vector identity, $\nabla \times \nabla \times \boldsymbol{\omega} = \nabla(\nabla \cdot \boldsymbol{\omega}) - \nabla^2 \boldsymbol{\omega}$, the Laplacian on the right-hand side of Equation (1) can be rewritten as

$$\nabla^2 \boldsymbol{\omega} = -\nabla \times \nabla \times \boldsymbol{\omega} \tag{6}$$

The difference between these two forms is that the 'curl form' of each vorticity transport equations contains a 2D Laplacian for the actual vorticity component and mixed derivative terms with the two other vorticity components (see e.g. the transport equations in cylindrical co-ordinates Equations 9–11), whereas the 'Laplacian form' contains derivatives in all space directions but no mixed derivatives. Solving all three vorticity transport equations simultaneously, as shown by Guj and Stella [5] and Shen and Ta Phuoc [6], preserves the divergence of the vorticity. Taking the divergence of the vorticity transport equations in 'curl form' and using the operator identity $\nabla \cdot (\nabla \times \mathbf{f}) = 0$, we get

$$\frac{\partial}{\partial t} (\nabla \cdot \boldsymbol{\omega}) = 0 \tag{7}$$

Thus, if the vorticity is solenoidal at time $t = t_o$, it will remain so at later time and for this reason we used the 'curl-form'.

The advantage of the vorticity–velocity formulation is that the vorticity is determined directly from the equations with the same accuracy as the velocity. This latter may be of importance when studying vortex dominated flows where the vorticity field is known to play an important role in the dynamics of organized flow structures. Furthermore, as discussed by Speziale [7], non-inertial effects enter only into the solution through the implementation

of initial and boundary conditions. For many practical applications, however, the pressure is needed, e.g. to determine the forces on a construction. Also, there exists very little experience using eddy viscosity turbulence models in 3D vorticity–velocity CFD models.

In the discretized 3D vorticity–velocity formulation, the Cauchy–Riemann type equations for the velocity field constitute an overdetermined system. This problem can be overcome by applying the curl operator on the vorticity definition equation and exploiting the continuity equation to obtain three Poisson equations, one for each of the components of the velocity vector.

$$\nabla^2 \mathbf{V} = -\nabla \times \boldsymbol{\omega} \tag{8}$$

The Poisson equation formulation, however, does not guarantee a solenoidal velocity field, and we are left with the same problem as in the primitive variables formulation. In spite of this, in many studies dealing with 3D vorticity–velocity formulations the Poisson equations were employed to determine the velocity components (e.g. References [5, 8–15]). Recently, various versions of the Poisson equations using the continuity equation as a third equation have been employed to obtain a solenoidal velocity field [6, 16, 17]. But only few investigations have treated the Cauchy–Riemann type system directly [18–20]. Osswald *et al.* [18] devised a technique that eliminated the linear dependent discretized C–R equations to balance the number of equations to the number of unknowns. Further, they developed a direct inversion algorithm on the remaining equations which, however, required access to a large amount of computer storage. Gatski *et al.* [19] employed an iterative least squares method (Kaczmarz algorithm) on the entire overdetermined system of discretized C–R equations. The convergence of this method is, however, known to be slow and depends strongly on the relaxation parameter. This was shown in Hansen [21], who instead applied a conjugate gradient method to solve the least squares problem (see Section 3.3).

Up to now, the vorticity–velocity formulation of the 3D Navier–Stokes equations has only been employed on a limited number of flow cases, mostly described in Cartesian co-ordinates. One recent exception, however, is the general formulation of Bertagnolio and Daube [22].

In the past years, the authors have derived a general methodology for the solution of the vorticity–velocity form of the Navier–Stokes equations based on solving the Cauchy–Riemann equations, as described in Hansen *et al.* [20]. The algorithm presented herein is a further development of this method in cylindrical co-ordinates that also treats the polar singularity at the axis of the cylindrical domain.

The paper is organized as follows. In Section 2 the governing equations and their boundary conditions in cylindrical co-ordinates are presented. Particular attention is given here to the polar singularity that appears at the axis of the cylindrical domain. Section 3 describes the numerical technique employed to solve the equations. In Section 4 results are shown and compared to measurements for the cases of a developing flow in a pipe and a rotating flow in a closed cylinder. Both axisymmetric and non-axisymmetric (3D) flows are treated. Finally, in Section 5 conclusions and recommendation for future works are outlined.

2. GOVERNING EQUATIONS AND BOUNDARY CONDITIONS

We now consider a cylindrical co-ordinate system (r, θ, z) with the velocity vector $\mathbf{V} = (V_r, V_\theta, V_z)$ and the vorticity $\boldsymbol{\omega} = (\omega_r, \omega_\theta, \omega_z)$. For each vorticity component, the vorticity transport

equations are written in curl-form as follows:

$$\frac{\partial(r\omega_r)}{\partial t} - \nu\frac{\partial}{\partial\theta}\left[\frac{1}{r}\frac{\partial\omega_r}{\partial\theta} - \frac{1}{r}\frac{\partial(r\omega_\theta)}{\partial r}\right] - \nu\frac{\partial}{\partial z}\left[r\frac{\partial\omega_r}{\partial z} - r\frac{\partial\omega_z}{\partial r}\right] = \frac{\partial}{\partial\theta}[\omega_\theta V_r - \omega_r V_\theta] + \frac{\partial}{\partial z}[r\omega_z V_r - r\omega_r V_z] \tag{9}$$

$$\frac{\partial\omega_\theta}{\partial t} - \nu\frac{\partial}{\partial r}\left[\frac{1}{r}\frac{\partial(r\omega_\theta)}{\partial r} - \frac{1}{r}\frac{\partial\omega_r}{\partial\theta}\right] - \nu\frac{\partial}{\partial z}\left[\frac{\partial\omega_\theta}{\partial z} - \frac{1}{r}\frac{\partial\omega_z}{\partial\theta}\right] = \frac{\partial}{\partial r}[\omega_r V_\theta - \omega_\theta V_r] + \frac{\partial}{\partial z}[\omega_z V_\theta - \omega_\theta V_z] \tag{10}$$

$$\frac{\partial(r\omega_z)}{\partial t} - \nu\frac{\partial}{\partial r}\left[r\frac{\partial\omega_z}{\partial r} - r\frac{\partial\omega_r}{\partial z}\right] - \nu\frac{\partial}{\partial\theta}\left[\frac{1}{r}\frac{\partial\omega_z}{\partial\theta} - \frac{\partial\omega_\theta}{\partial z}\right] = \frac{\partial}{\partial r}[\omega_r r V_z - r\omega_z V_r] + \frac{\partial}{\partial\theta}[\omega_\theta V_z - \omega_z V_\theta] \tag{11}$$

The vorticity components are defined as

$$\omega_r = \frac{1}{r}\frac{\partial V_z}{\partial\theta} - \frac{\partial V_\theta}{\partial z} \tag{12}$$

$$\omega_\theta = \frac{\partial V_r}{\partial z} - \frac{\partial V_z}{\partial r} \tag{13}$$

$$\omega_z = \frac{1}{r}\frac{\partial(rV_\theta)}{\partial r} - \frac{1}{r}\frac{\partial V_r}{\partial\theta} \tag{14}$$

and the corresponding continuity equation reads

$$\frac{\partial}{\partial r}(rV_r) + \frac{\partial V_\theta}{\partial\theta} + r\frac{\partial V_z}{\partial z} = 0 \tag{15}$$

The calculation domain is limited by $r\in[0,R]$, $\theta\in[0,2\pi]$ and $z\in[0,L_z]$ where R denotes the radius to the lateral boundary, L_z is the length of the domain and θ is the azimuthal angle defined positive counter-clockwise. In the flow cases that will be considered in the following the lateral boundary is always a solid wall, whereas the plane defined by $z=0$ is either a fixed solid wall or an inflow plane and the endplane at $z=L_z$ is either a (translating or rotating) solid wall or an outflow plane. At solid walls no-slip conditions are assumed for all velocity components. Boundary conditions for the vorticity components are constructed from the definition equations, Equations (12)–(14). To summarize, the boundary conditions for velocity and vorticity are defined as follows:

Lateral boundary ($r=R,\ 0\leqslant\theta\leqslant 2\pi,\ 0\leqslant z\leqslant L_z$):

$$V_r=0,\quad V_\theta=0,\quad V_z=0$$

$$\omega_r=0,\quad \omega_\theta=-\frac{\partial V_z}{\partial r},\quad \omega_z=\frac{1}{R}\frac{\partial(rV_\theta)}{\partial r}$$

Endwalls ($0\leqslant r\leqslant R,\ 0\leqslant\theta\leqslant 2\pi,\ z=0$ or $z=L_z$):

$$V_r=\tilde{V}_r,\quad V_\theta=\tilde{V}_\theta,\quad V_z=0$$

$$\omega_r=-\frac{\partial V_\theta}{\partial z},\quad \omega_\theta=\frac{\partial V_r}{\partial z},\quad \omega_z=0$$

Inflow boundary ($0\leqslant r\leqslant R,\ 0\leqslant\theta\leqslant 2\pi,\ z=0$):

$$V_r=0,\quad V_\theta=0,\quad V_z=\tilde{V}_z$$

$$\omega_r=\frac{1}{r}\frac{\partial\tilde{V}_z}{\partial\theta}-\frac{\partial V_\theta}{\partial z},\quad \omega_\theta=\frac{\partial V_r}{\partial z}-\frac{\partial\tilde{V}_z}{\partial r},\quad \omega_z=0$$

Outflow boundary ($0\leqslant r\leqslant R,\ 0\leqslant\theta\leqslant 2\pi,\ z=L_z$):

$$\frac{\partial V_r}{\partial z}=0,\quad \frac{\partial V_\theta}{\partial z}=0,\quad \frac{\partial V_z}{\partial z}=0$$

$$\omega_r=\frac{1}{r}\frac{\partial V_z}{\partial\theta}-\frac{\partial V_\theta}{\partial z},\quad \omega_\theta=\frac{\partial V_r}{\partial z}-\frac{\partial V_z}{\partial r},\quad \omega_z=\frac{1}{r}\frac{\partial(rV_\theta)}{\partial r}-\frac{1}{r}\frac{\partial V_r}{\partial\theta}$$

The boundary conditions are imposed such that the velocity conditions are used in the C–R type system, Equations (12)–(15), and the vorticity conditions are employed in the transport equations, Equations (9)–(11). A tilde means that the variable is given as a prescribed constant. As the transport equation are written in curl-form, no boundary conditions are necessary for the solution of the ω_z-transport equation at the boundaries $z=0$ and L_z. However, as mixed derivatives of ω_z appear in the two other transport equations, it is necessary to attribute some value to ω_z at the in- and out-flow planes. Furthermore, it should be noted that although no boundary conditions are needed explicitly for V_r and V_θ at in- and out-flow, V_r and V_θ are imposed implicitly in the boundary conditions for the transport equations.

Periodic boundary conditions are employed for all variables in the θ-direction.

At the axis of the cylindrical domain, $r=0$, a polar singularity appears. To overcome the difficulty, we introduce Cartesian components (V_{xo}, V_{yo}) and $(\omega_{xo}, \omega_{yo})$ as unknowns at the axis. The relations between the cylindrical and Cartesian variables read

$$V_r=V_x\cos\theta+V_y\sin\theta \tag{16}$$

$$V_\theta=V_y\cos\theta-V_x\sin\theta \tag{17}$$

$$\omega_r=\omega_x\cos\theta+\omega_y\sin\theta \tag{18}$$

$$\omega_\theta=\omega_y\cos\theta-\omega_x\sin\theta \tag{19}$$

For the z-direction components, the velocity V_z is well defined and no problem is posed. The vorticity ω_z, however, is singular. To overcome the difficulty, ω_z is transformed in Cartesian co-ordinates by using the relations (16)–(17) and

$$x = r\cos\theta$$

$$y = r\sin\theta$$

Then Equation (14) takes the Cartesian form, ($\omega_z = \partial V_y/\partial x - \partial V_x/\partial y$), on the axis.

The actual implementation of these terms in the discretized system of equations will be described in the next section.

3. NUMERICAL METHOD

The computational domain is defined by the mesh points $r_i = i\delta r$, $\theta_j = (j-1)\delta\theta$ and $z_k = (k-1)\delta z$ where $i \in [0, N_R]$, $j \in [1, N_T]$, $k \in [1, N_Z]$, and $\delta r = R/N_R$, $\delta\theta = 2\pi/(N_T - 2)$, $\delta z = L_z/(N_Z - 1)$. Thus, in the r-direction $i = 0$ corresponds to the axis of the cylindrical domain, $r_o = 0$, and the overlapping of grid points in the θ-direction ensures the periodicity of the involved variables, i.e. $f\,|_{j=1} = f\,|_{j=N_T-1}$ and $f\,|_{j=N_T} = f\,|_{j=2}$. To advance the solution in time requires two steps. First, the vorticity field $\boldsymbol{\omega}$ is found by solving the vorticity transport equations, Equations (9)–(11), with given velocity field $\mathbf{V}$. Next, the new velocity field $\mathbf{V}$ is found by solving the C–R system, Equations (12)–(15), with $\boldsymbol{\omega}$ given from the previous step. Finally, the boundary conditions for the vorticity are updated from the definition equations and the solution procedure is progressed to the next time step.

The governing equations are solved by employing a standard second-order accurate finite difference technique for the transport equations and a box scheme for the Cauchy–Riemann system.

3.1. Solution of the transport equations

To advance the transport equations, Equations (9)–(11), in time, we employ a semi-implicit Crank–Nicolson type scheme for the diffusion terms and an explicit Adams–Bashforth extrapolation discretization for the convection-stretching terms. Let δt denote the time increment, $\mathbf{L}_\mathrm{d}$ be the diffusion operator and $\mathbf{L}_\mathrm{c}$ the convection-stretching operator, the transport equations are discretized in a Helmholtz equation form:

$$\boldsymbol{\omega}^{n+1} - \frac{\delta t}{2}\mathbf{L}_\mathrm{d}^{n+1}(\boldsymbol{\omega}) = \boldsymbol{\omega}^n + \frac{\delta t}{2}[\mathbf{L}_\mathrm{d}^n(\boldsymbol{\omega}) - 3\mathbf{L}_\mathrm{c}^n(\boldsymbol{\omega}) + \mathbf{L}_\mathrm{c}^{n-1}(\boldsymbol{\omega})] \tag{20}$$

To ensure that the discrete vorticity obeys the constraint $\nabla \cdot \boldsymbol{\omega} = 0$, the three Helmholtz equations are solved simultaneously on a staggered grid as shown in Figure 1. The collocation points of the vorticity components are defined as follows (see Figure 1), so that only the normal vorticity component is stored on each cell face:

- The vorticity component ω_r is defined at nodes $(i\delta r, (j+1/2)\delta\theta, (k+1/2)\delta z)$ for $1 \leqslant i \leqslant N_R$, $1 \leqslant j \leqslant N_T$, $1 \leqslant k \leqslant N_Z - 1$.

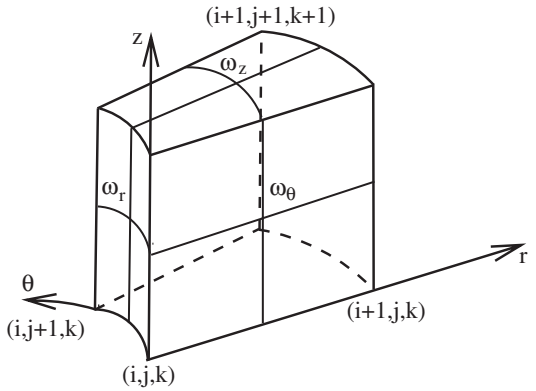

Figure 1. Location of staggered vorticity vector.

- The vorticity component ω_θ is defined at nodes $((i+1/2)\delta r,\ j\delta\theta,(k+1/2)\delta z)$ for $0\leqslant i\leqslant N_R-1,\ 1\leqslant j\leqslant N_T,\ 1\leqslant k\leqslant N_Z-1$.
- The vorticity component ω_z is defined at nodes $((i+1/2)\delta r,(j+1/2)\delta\theta,k\delta z)$ for $0\leqslant i\leqslant N_R-1,\ 1\leqslant j\leqslant N_T,\ 1\leqslant k\leqslant N_Z$.

The spatial discretization is carried out at the same locations by employing standard second-order accurate central differences. The velocity vector is not staggered, but located on the vertices in the grid.

3.2. *Polar singularity of the transport equations*

The ω_r-equation is discretized at the points $(i,j+\frac{1}{2},k+\frac{1}{2})$. At the centre axis $(i=0)$, all terms vanish and the equation is identically satisfied. At the first points away from the centre axis, the equation contains no radial derivatives. Hence, all the variables needed are well defined and the equation can be solved without any problems.

The ω_θ-equation is discretized at the points $(i+\frac{1}{2},j,k+\frac{1}{2})$. At the first points $(i=0)$, the equation contains a singular term arising from the radial derivative of the diffusion term, $(1/r\partial(r\omega_\theta)/\partial r - 1/r\partial\omega_r/\partial\theta)\ |_{r=0}$. To overcome the difficulty, it is transformed into Cartesian co-ordinates, $(\partial\omega_y/\partial x - \partial\omega_x/\partial y)\ |_{r=0}$. The second and last non-defined term is $(\omega_r V_\theta - \omega_\theta V_r)\ |_{r=0}$ which appears in the discretization of the radial derivative of the convection and stretching terms. This term is also transformed into Cartesian co-ordinates, taking the form, $(\omega_x V_y - \omega_y V_x)\ |_{r=0}$.

The ω_z-equation is discretized at the points $(i+\frac{1}{2},\ j+\frac{1}{2},k)$. At the first points to be discretized $(i=0)$, the same problem as in the ω_θ-equation occurs. In this case the difficult terms, $(r\partial\omega_z/\partial r - r\partial\omega_r/\partial z)\ |_{r=0}$ and $(r\omega_r V_z - r\omega_z V_r\ |_{r=0})$, both contain multiplication by r and they are simply put equal to zero.

In order to determine the values of ω_x and ω_y at the singular axis, we use two steps. First, the Cartesian components are evaluated at $r=r_1$ using the following two relations:

$$(\omega_x)_{1,j,k+1/2} = [((\omega_r)_{1,j+1/2,k+1/2} + (\omega_r)_{1,j-1/2,k+1/2})\cos\theta_j - ((\omega_\theta)_{3/2,j,k+1/2} + (\omega_\theta)_{1/2,j,k+1/2})\sin\theta_j]/2 \tag{21}$$

$$(\omega_y)_{1,j,k+1/2} = [((\omega_r)_{1,j+1/2,k+1/2} + (\omega_r)_{1,j-1/2,k+1/2}) \sin\theta_j + ((\omega_\theta)_{3/2,j,k+1/2} + (\omega_\theta)_{1/2,j,k+1/2}) \cos\theta_j]/2 \tag{22}$$

Next, the Cartesian components at $r=0$ are approximated as the average of the values at $r=r_1$:

$$(\omega_{x_o})_{k+1/2} = \frac{1}{N_T - 2} \sum_{j=2}^{N_T-1} (\omega_x)_{1,j,k+1/2} \tag{23}$$

$$(\omega_{y_o})_{k+1/2} = \frac{1}{N_T - 2} \sum_{j=2}^{N_T-1} (\omega_y)_{1,j,k+1/2} \tag{24}$$

In employing this procedure, all singular terms are now defined and the matrix of the transport equation is established. The matrix is solved by an iterative line-relaxation method which converges very fast.

Note that the treatment of the singular axis does not influence the divergence of the vorticity transport equations, such that the divergence of the vorticity ($\nabla \cdot \boldsymbol{\omega} = 0$) is conserved correctly.

3.3. Solution of the Cauchy–Riemann equations

The Cauchy–Riemann equations, Equations (12)–(15), constitute a set of four first order differential equations to be solved for the velocity (V_r, V_θ, V_z).

The discretization of the continuity equation, Equation (15), is based upon Gauss' theorem:

$$\int\int\int_v \nabla \cdot \mathbf{V}\, \mathrm{d}v = \int\int_S \mathbf{V} \cdot \mathbf{n}\, \mathrm{d}S \tag{25}$$

where v denotes the volume of the cell, $\mathbf{n}$ is the outward normal vector and dS is the incremental of the surface bounding the cell. Employing Equation (25) and approximating Equation (15) for a cell, as shown in Figure 1, yields:

$$\frac{(rV_r)_{i+1,j+1/2,k+1/2} - (rV_r)_{i,j+1/2,k+1/2}}{\Delta r} + \frac{(V_\theta)_{i+1/2,j+1,k+1/2} - (V_\theta)_{i+1/2,j,k+1/2}}{\Delta\theta} + r_{i+1/2} \frac{(V_z)_{i+1/2,j+1/2,k+1} - (V_z)_{i+1/2,j+1/2,k}}{\Delta z} = 0 \tag{26}$$

Since the velocities are located at the vertices, the term $(V_z)_{i+1/2,j+1/2,k}$ is found as the mean of the values for V_z at the vertices $(i,j,k),(i+1,j,k),(i+1,j+1,k)$ and $(i,j+1,k)$.

The discretization of the vorticity definition equations (12)–(14) is based upon Stokes' theorem:

$$\oint \mathbf{V} \cdot \mathrm{d}\mathbf{l} = \int\int_S (\nabla \times \mathbf{V}) \cdot \mathbf{n}\, \mathrm{d}S = \int\int_S \boldsymbol{\omega} \cdot \mathbf{n}\, \mathrm{d}S \tag{27}$$

where $\mathrm{d}\mathbf{l}$ is the infinitesimal tangent vector to the closed curve enclosing the open surface denoted S. In cylindrical co-ordinates it is noted that the radial vorticity component ω_r is normal to the plane $i=$constant, the tangential vorticity component ω_θ is normal to the plane

$j=$constant and the axial vorticity component ω_z is normal to the plane $k=$constant. This is illustrated in Figure 1 and makes the evaluation of Equation (27) straightforward.

As an example, Equation (27) is used at a plane $i=$const to derive the discrete ω_r definition equation:

$$r_i\Delta\theta(V_\theta)_{i,j+1/2,k}+\Delta z(V_z)_{i,j+1,k+1/2}-r_i\Delta\theta(V_\theta)_{i,j+1/2,k+1}-\Delta z(V_z)_{i,j,k+1/2}$$
$$=\Delta z\Delta\theta r_i(\omega_r)_{i,j+1/2,k+1/2} \tag{28}$$

which, alternatively, is written as follows:

$$\frac{(V_z)_{i,j+1,k+1/2}-(V_z)_{i,j,k+1/2}}{\Delta\theta}-r_i\frac{(V_\theta)_{i,j+1/2,k+1}-(V_\theta)_{i,j+1/2,k}}{\Delta z}=(r\omega_r)_{i,j+1/2,k+1/2} \tag{29}$$

By evaluating Equation (27) at the planes $j=$const and $k=$const, respectively, in a similar way the ω_θ and ω_z definition equations are derived as follows:

$$\frac{(V_r)_{i+1/2,j,k+1}-(V_r)_{i+1/2,j,k}}{\Delta z}-\frac{(V_z)_{i+1,j,k+1/2}-(V_z)_{i,j,k+1/2}}{\Delta r}=(\omega_\theta)_{i+1/2,j,k+1/2} \tag{30}$$

$$\frac{(rV_\theta)_{i+1,j+1/2,k}-(rV_\theta)_{i,j+1/2,k}}{\Delta r}-\frac{(V_r)_{i+1/2,j+1,k}-(V_r)_{i+1/2,j,k}}{\Delta\theta}=(r\omega_z)_{i+1/2,j+1/2,k} \tag{31}$$

As written before the velocities are stored at the grid points and values not evaluated explicitly at the node points are determined by averaging of neigbouring points. For example:

$$(V_\theta)_{i,j+1/2,k}=\tfrac{1}{2}\left((V_\theta)_{i,j+1,k}+(V_\theta)_{i,j,k}\right) \tag{32}$$

Note that the discretized Cauchy–Riemann equations constitute an overdetermined linear system of equations.

The singularity at $r=0$ is overcome by replacing $V_r(r=0)$ and $V_\theta(r=0)$ with the Cartesian components V_{x_o} and V_{y_o}, as shown in Equations (16) and (17). This, of course, yields more equations than unknowns at the centre axis. But, as we in all cases are dealing with an overdetermined system, this does not pose any problems in the solution procedure.

The discretized system of equations is expressed as

$$\underline{\underline{A}}\ \underline{V}=\underline{b} \tag{33}$$

where $\underline{\underline{A}}$ is a $m\times q$ coefficient matrix, $\underline{V}$ is a vector containing q unknown velocity components and the right-hand vector $\underline{b}$ contains m elements. This system is overdetermined. To solve the system, Gatski *et al.* [19] used an iterative least squares method (Kaczmarz algorithm). However, the convergence of this method is slow. In order to increase the convergence rate, a new iterative least squares method is developed. Applying twice a diagonal matrix $\underline{\underline{D}}$ and the transpose matrix $\underline{\underline{A}}^{\mathrm{T}}$, we get the normal system of equations as

$$(\underline{\underline{A}}^{\mathrm{T}}\underline{\underline{D}}\ \underline{\underline{D}}\ \underline{\underline{A}})\underline{V}=\underline{\underline{A}}^{\mathrm{T}}\underline{\underline{D}}\ \underline{\underline{D}}\ \underline{b} \tag{34}$$

The diagonal matrix $\underline{\underline{D}}$ is chosen so that it weights the equations equally. Hence, the elements on the diagonal of $\underline{\underline{D}}$ are $d_{ii}=||a_i\ ||_2^{-1}$, where a_i denotes the i'th row of $\underline{\underline{A}}$. The solution of Equation (34) is found by applying a standard conjugate gradient method. According to

Oppe *et al.* [23] this method is denoted CGNR. To test the ability of the developed method, a comparative study between the Kaczmarz and the CGNR methods was made by Hansen [21]. It was shown that the CGNR method is superior and gives good results.

The definition of vorticity, Equations (16)–(18), is used to determine the boundary conditions for the vorticity transport equations. Therefore all the discretized vorticity definition equations (33)–(35) touching a boundary are ignored when solving the overdetermined discretized Cauchy–Riemann equations. None of the discretized continuity equations are ignored. This method for solving the overdetermined system of discretized Cauchy–Riemann equations is consistent with the analytical formulation stating that only the normal velocity is needed on the boundary. It was tested that specifying the vorticity vector as $\omega_r = 0$, $\omega_\theta = 0$ and $\omega_z = 2\Omega$ yielded a solid body rotation $V_\theta = \Omega r$, $V_r = V_z = 0$.

4. NUMERICAL RESULTS

To validate the developed algorithm and the proposed boundary conditions, results are presented for the cases of a developing flow in a pipe and a rotating flow in a closed cylinder where the fluid motion is initiated either by letting an endwall rotate with a constant angular velocity or by letting it be subject to a translatory motion. The reason for this choice is that experimental results are available and that both axisymmetric and non-axisymmetric behaviour can be analysed.

4.1. Developing flow in a pipe

As a first test case we calculate a developing flow in a pipe. At the entrance of the pipe, the axial velocity distribution is assumed to be constant or to vary linearly with y. In cylindrical co-ordinates this is written as

$$V_z = V_o \left(1 + \delta \frac{r}{R} \sin\theta\right) \tag{35}$$

where V_o is the mean axial velocity and δ is a parameter that determine the rate of shear:

$$\delta = R \frac{\partial}{\partial y} \left(\frac{V_z}{V_o}\right)$$

Thus, putting δ equal to zero corresponds to axisymmetric flow conditions, whereas $\delta \neq 0$ gives rise to non-axisymmetric flow behaviour. Based on mean axial velocity and pipe radius, the Reynolds number is defined as $Re = V_o R/v$.

At first, results for $\delta = 0$ are compared to the measurements of Nikuradse (reproduced in Reference [24]). In this case it is known from measurements and approximative analytical studies that the axial length, L, necessary to make the flow fully developed is determined as $L = 0.24R \cdot Re$. In the calculation, we put $Re = 20$ and $L_z = 5R$ which ensures that the flow is fully developed at the outflow boundary. The equations are discretized by employing a grid spacing of $N_R \times N_T \times N_Z = 30 \times 30 \times 101$ node points.

In Figure 2, calculated axial velocity distributions are compared with measured values as function of the dimensionless distance, z/Re, at various $r =$ constant lines. It is noted that the solution remains axisymmetric and thus independent of the θ-co-ordinate. Over most of the pipe the calculations are observed to be in good agreement with the experimental values.

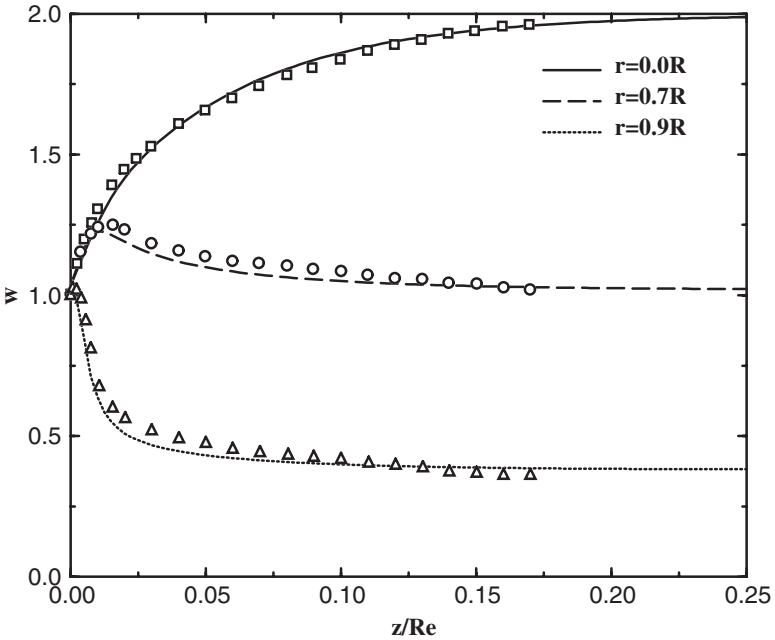

Figure 2. Axial velocity distributions of the developing flow in a pipe with $\delta = 0$, compared with measured values at various radial positions.

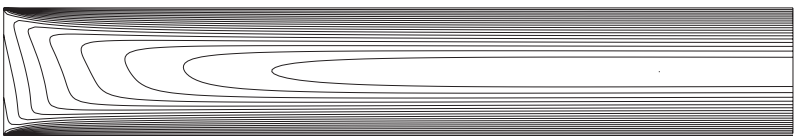

Figure 3. Axial velocity distribution in $y - z$ plane of the developing flow in a pipe with $\delta = 0.2$.

To analyse the ability of the code to calculate non-axisymmetric flows, a computation is performed setting $\delta = 0.2$. The inflow is thus defined by a plane shear flow which, under the influence of viscous forces, gradually becomes parabolic. It should be recalled here that only the axial velocity is fixed at the inflow boundary, whereas the two other velocity components are determined as a result of the calculation. Furthermore, as both ω_r and ω_θ are non-zero, axial vorticity will be created from vortex stretching, resulting in the generation of a swirling motion. In Figure 3, an iso-plot of the calculated axial velocity distribution is depicted in the $y - z$ plane defined by $x = 0$ (corresponding to the two half-planes $\theta = \pi/2$ and $\theta = -\pi/2$). It is seen that, in the immediate vicinity of the inflow boundary, the flow is forced towards the bottom of the plane. It is interesting to note that flow passes continuously through the polar singularity. In Figures 4 and 5, secondary flow velocity components, V_x and V_y, are shown in the two planes defined by $k = 11$ and 21, respectively. The flow is observed to perform a swirling motion and also here no anomalies appear at the polar axis. Finally, Figure 6 depicts the iso-surface plot of the streamwise vorticity, ω_z, to demonstrate that the inflow conditions create a ω_z-field which is concentrated at the upper part just downstream of the entrance.

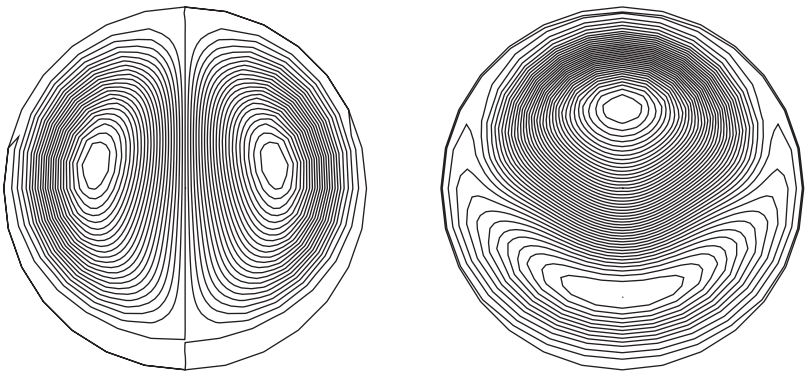

Figure 4. Secondary velocity components, V_x and V_y, of the developing flow in a pipe with $\delta = 0.2$ at $k = 11$.

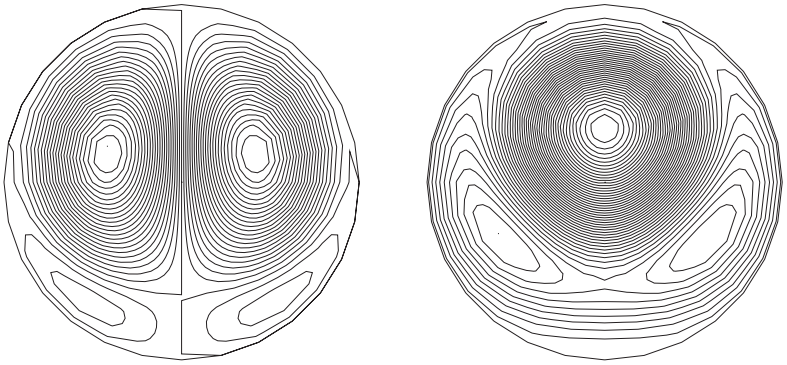

Figure 5. Secondary velocity components, V_x and V_y, of the developing flow in a pipe with $\delta = 0.2$ at $k = 21$.

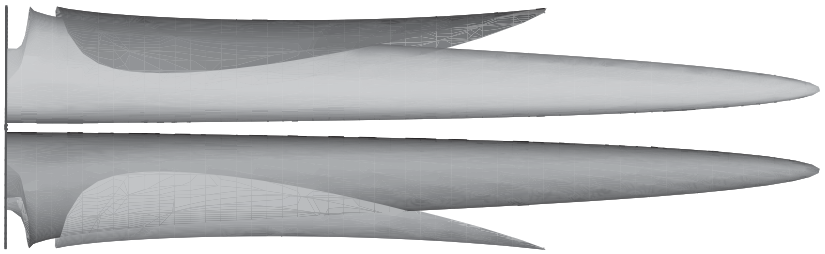

Figure 6. Iso-surface plot of the streamwise vorticity, $\omega_z = -0.02$ and 0.02, of the developing flow in a pipe with $\delta = 0.2$.

4.2. *Flow in a closed cylinder*

The second test case concerns a swirling flow in a closed cylinder, where one of the endwalls rotates with a constant angular velocity, Ω, or translates with a constant velocity, V_o. Letting dimensions be given by the height, H, and the radius, R, the flow conditions are uniquely defined by the aspect ratio, $\lambda = H/R$, and the Reynolds number, $Re = \Omega R^2/v$ or $V_o R/v$.

4.2.1. Rotating flow Due to the rotation, a boundary layer on the rotating top wall centrifuges the fluid outwards to the cylinder wall, from where it spirals in the direction of the fixed bottom wall. When a fluid element reaches the bottom wall, it is attracted towards the axis of the cylinder, along which a concentrated vortex is formed. Depending on the Reynolds number and aspect ratio, this vortex may develop stagnation points and closed stream surfaces, a phenomenon that has been interpreted as vortex breakdown.

The first visualizations of this flow configuration were carried out by Vogel [25]. Later, these visualizations were supplemented by LDA measurements by Ronnenberg [26] and Michelsen [27]. The first systematic study of the flow structures was performed experimentally by Escudier [28], who showed that up to three recirculating bubbles on the axis were observed as λ and Re were changed.

Assuming axisymmetric flow conditions, some of the experimental findings have been confirmed numerically by e.g. Lugt and Abboud [29], Daube and Sørensen [30] and Lopez [31].

To validate the developed algorithm, a computation of a cylinder with aspect ratio, $\lambda = 1$, and Reynolds number, $Re = 1800$, is performed, as in this particular case detailed LDA measurements have been performed by Michelsen [27]. The calculations were carried out by employing a grid of $N_R \times N_T \times N_Z = 20 \times 30 \times 31$ node points.

Figure 7 compares computed tangential and radial velocity distributions along $r = 0.7$, 0.8 and 0.9 constant lines with the measurements of Michelsen. The solutions are found to be independent of the θ-direction and in excellent agreement with the measurements over most of the flow field. Near the boundaries, however, some deviations are seen. It should be noted, however, that the same deviations were found in earlier comparisons where axi-symmetric algorithms were utilized [27, 32].

4.2.2. Translating flow In order to verify the treatment of the centre axis, a computation is performed for the case of the flow in a closed cylinder where the top cover is translated with a constant velocity, V_o. The boundary condition on the top wall becomes

$$V_r = V_o \cos\theta$$

$$V_\theta = -V_o \sin\theta$$

Due to the translation, a boundary layer is formed on the top wall and the fluid is moved from left to right (see Figure 8). When a fluid element reaches the lateral wall, it is forced towards to the fixed bottom wall and performs a motion similar to the flow in a driving cavity. Due to the cylindrical geometry, however, a secondary flow is generated and the flow becomes fully 3D.

In Figure 8 velocity vectors are shown in the x–z plane. From the figure it is seen that flow passes continuously through the polar singularity and no effects from the treatment at the centre axis can be observed. The corresponding velocity vectors in the y–z plane are shown

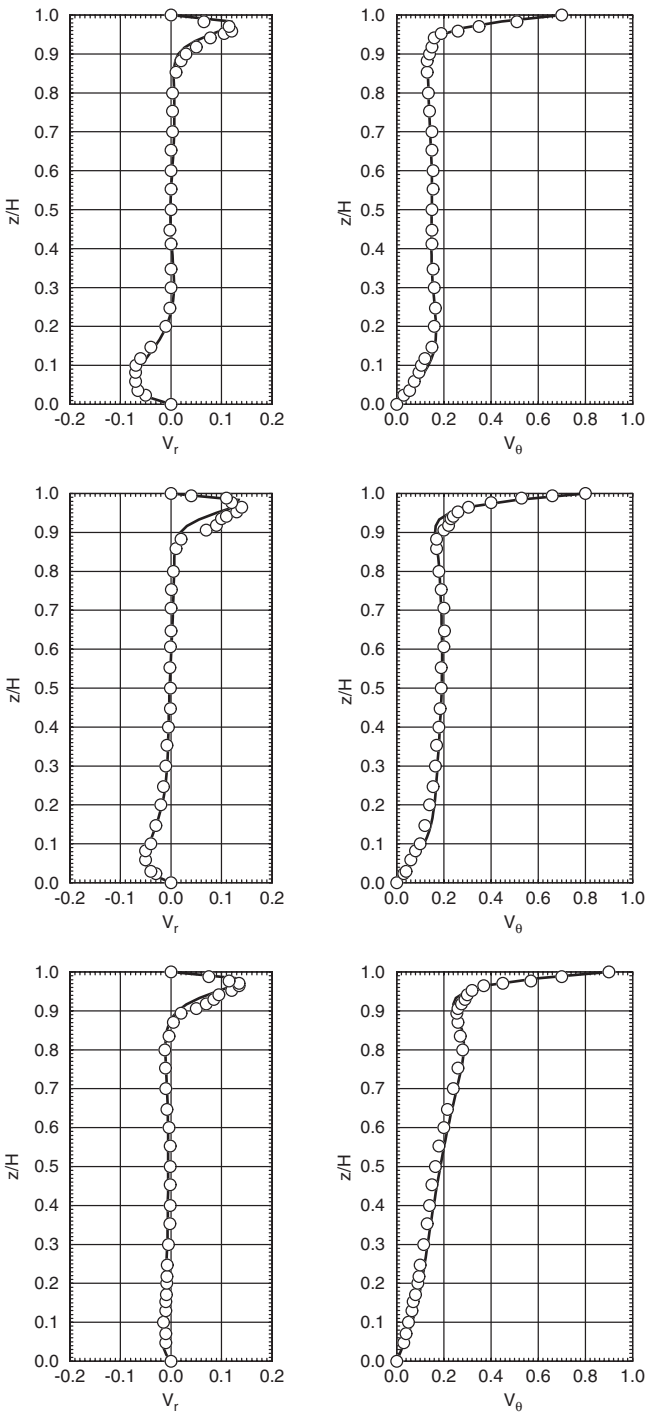

Figure 7. Velocity distributions V_r (left) and V_θ (right) of the rotating flow in a closed cylinder at $r = 0.7$ (top), 0.8 (middle) and 0.9 (bottom), compared with measurements [27].

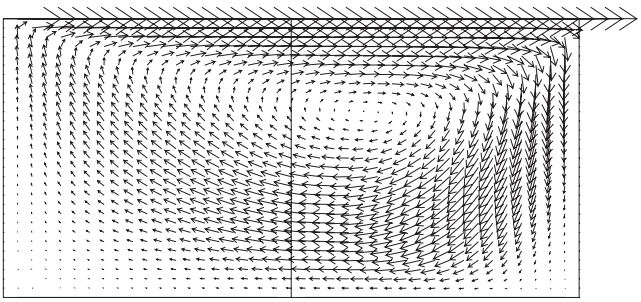

Figure 8. Velocity vectors in the x–z plane of the translating flow in a closed cylinder at $Re = 100$.

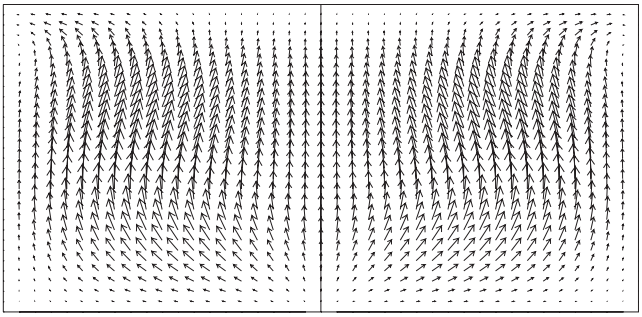

Figure 9. Velocity vectors in the y–z plane of the translating flow in a closed cylinder at $Re = 100$.

in Figure 9. In this plane, the flow is symmetrical. Finally, in Figure 10a 3D view of the iso-surface plot of the absolute vorticity, demonstrates that the computed vorticity is smooth everywhere in the flow domain.

5. CONCLUSION

A finite difference method is presented for solving the 3D Navier–Stokes equations in vorticity–velocity form using cylindrical co-ordinates. The method involves solving simultaneously all three vorticity transport equations in 'curl-form' to numerically ensure a solenoidal vorticity field. The velocity field is determined by solving the discretized Cauchy–Riemann equations using a conjugate gradient method to the normal equations.

A technique to treat the singularity at the polar axis is proposed. For the vorticity field, a staggered grid is used and singular terms are transformed into Cartesian co-ordinates. For the velocity equations, the problem is solved by implicitly introducing Cartesian components at the centre axis.

The method is successfully validated by computing the developing laminar flow in a pipe and the flow in a closed cylinder, where one of the end lids is rotating. Both cases are in good agreement with experimental data. Further, to verify the treatment of the polar centre axis, the developing laminar flow in a pipe was recomputed, but with a non-axisymmetric

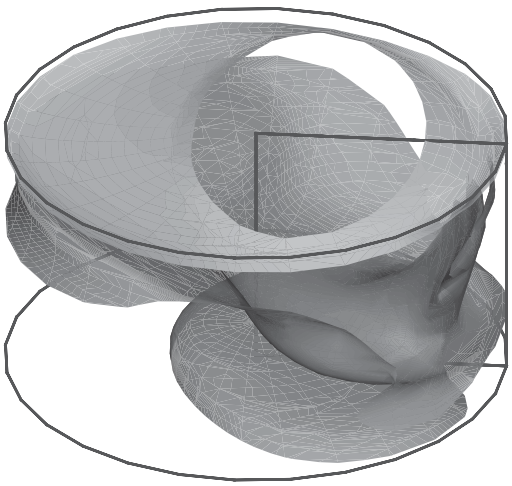

Figure 10. Iso-surface plot of the absolute vorticity, $|| \boldsymbol{\omega} ||_2 = 1$ and 6, of the translating flow in a closed cylinder at $Re = 100$.

inflow. At some distance downstream, the flow becomes axisymmetric with the well known parabolic axial velocity profile. To go from the non-axisymmetric inflow to the fully developed axisymmetric solution the flow has to cross the centre axis. It is checked that this occurs smoothly for both the vorticity and velocity field. Also, the closed cylinder was recalculated, but now the end lid is translated. Due to friction, fluid is dragged in the direction of the moving lid until it reaches an endwall and is forced away from the lid and then back in the opposite direction of the moving lid. Again it was demonstrated that the flow past the centre axis occurs smoothly.

REFERENCES

1. Patankar SV. *Numerical Heat Transfer and Fluid Flow*. Hemisphere: New York, 1980.
2. Issa RI. Solution of the implicitly discretised fluid flow equations by operator-splitting. *Journal of Computational Physics* 1985; **62**:40.
3. Chorin AJ. Numerical solution of the Navier–Stokes equations. *Mathematics of Computation* 1968; **22**:745.
4. Temam R. *Archive for Rational Mechanics and Analysis* 1969; **32**:377.
5. Stella F, Guj G. Vorticity–velocity formulation in the computation of flows in multiconnected domains. *International Journal for Numerical Methods in Fluids* 1989; **9**:1285.
6. Shen WZ, Ta Phuoc Loc. Numerical method for unsteady 3D Navier–Stokes equations in velocity–vorticity form. *Computers and Fluids* 1997; **26**(2):193.
7. Speziale CG. On the advantages of the vorticity–velocity formulation of the equations of fluid dynamics. *Journal of Computational Physics* 1987; **73**:476.
8. Dennis SCK, Ingham DB, Cook RN. Finite-difference methods for calculating steady incompressible flows in three dimensions. *Journal of Computational Physics* 1979; **33**:325.
9. Daube O, Guermond JL, Sellier A. Sur la formulation vitesse-tourbillon des equations de Navier–Stokes en écoulement incompressible. *Comptes Rendus de l'Academie des Sciences Paris* 1991; **313**(II):377.
10. Fasel H. Investigation of the stability of boundary layers by a finite-difference model of the Navier–Stokes equations. *Journal of Fluid Mechanics* 1976; **78**:355.
11. Farouk B, Fusegi T. A coupled solution of the vorticity–velocity formulation of the incompressible Navier–Stokes equations. *International Journal for Numerical Methods in Fluids* 1985; **5**:1017.
12. Toumi A, Ta Phuoc Loc. Numerical study of three dimensional viscous incompressible flow by vorticity and velocity formulation. In *Proceedings of the Fifth International Conference on Numerical Methods in Laminar and Turbulent Flows*, *Montreal*, Canada, Taylor C *et al.* (eds). Pineridge Press: Swansea, UK, 1987, 595.

13. Napolitano M, Pascazio G. A numerical-method for velocity vorticity Navier–Stokes equations in 2-dimensions and 3-dimensions. *Computer and Fluids* 1991; **19**(3–4):489.
14. Liu CH. Numerical solution of three-dimensional Navier–Stokes equations by a velocity–vorticity method. *International Journal for Numerical Methods in Fluids* 2001; **35**:533–557.
15. Wong KL, Baker AJ. A 3D incompressible Navier–Stokes velocity–vorticity weak form finite element algorithm. *International Journal for Numerical Methods in Fluids* 2002; **38**:99–123.
16. Fontaine J, Loc T.-P. Etude numérique des sillages engendrés par une plaque d'envergure finie. *Comptes Rendus de l'Academie des Sciences Paris* 1995; **320**(II):581.
17. Wu XH, Wu JZ, Wu JM. Effective vorticity–velocity formulations for three-dimensional incompressible viscous flows. *Journal of Computational Physics* 1995; **122**:68–82.
18. Osswald GA, Ghia KN, Ghia U. A direct algorithm for solution of incompressible three dimensional unsteady Navier–Stokes equations. In *AIAA 8th Computational Fluid Dynamics Conference*, Honolulu, 1987; 408.
19. Gatski TB, Grosch CE, Rose ME. The numerical solution of the Navier–Stokes equations for 3-dimensional unsteady incompressible flows by compact schemes. *Journal of Computational Physics* 1989; **82**:298.
20. Hansen MOL, Sørensen JN, Barker VA. A numerical investigation of 3D flow past an infinite cylinder. In *Proceedings of the First European Computational Fluids Dynamics Conference*, Brussels, Hirsch Ch, Periaux J, Kordulla W (eds). Elsevier: Amsterdam, 1992, 375.
21. Hansen MOL. Vorticity–velocity formulation of the Navier–Stokes equations for aerodynamic flows. *Ph.D. Thesis*, AFM Report 94-07, Department of Fluid Mechanics, Technical University of Denmark, 1994.
22. Bertagnolio F, Daube O. Three-dimensional incompressible Navier–Stokes equations on non-orthogonal staggered grids using the velocity–vorticity formulation. *International Journal for Numerical Methods in Fluids* 1998; **28**(6):917.
23. Oppe TC, Joubert WD, Kincaid DR. A package for solving large sparse linear systems by various iterative methods. *Technical Report*, University of Texas, Austin, 1988.
24. Schlichting H. *Boundary Layer Theory*. McGraw-Hill: New York, 1979.
25. Vogel HU. Experimentelle ergebnisse über die laminare strömung in einem zylindrischen gehause mit darin rotierender scheibe. Bericht 6, Max-Planck-Institut für Strömungsforshung, Göttingen, 1968.
26. Ronnenberg B. Ein selbstjustierendes 3 komponenten LDA nach dem vergleichströhlverfahren, angewendt für untersuchungen in einer stationaren zylindersymmetrischen drehströhmung mit einem rüchströmgebiet. Bericht 20, Max-Planck Institut für Strömungsforshung, 1977.
27. Michelsen JA. Modeling of laminar incompressible rotating fluid flow. *Ph.D. Thesis*, AFM Report 86-07, Department of Fluid Mechanics, Technical University of Denmark, 1986.
28. Escudier MP. Observations of the flow produced in a cylindrical container by a rotating endwall. *Experiments in Fluids* 1984; **2**:189.
29. Lugt HJ, Abboud M. Axisymmetric vortex breakdown with and without temperature effects in a container with rotating lid. *Journal of Fluid Mechanics* 1987; **179**:179.
30. Daube O, Sørensen JN. Simulation numérique de l'écoulement périodique axisymmétrique dans une cavité cylindrique. *Comptes Rendus de l'Academie des Sciences Paris* 1989; **308**(II):463.
31. Lopez JM. Axisymmetric vortex breakdown, Part 1. Confined swirling flow. *Journal of Fluid Mechanics* 1990; **221**:533.
32. Sørensen JN, Ta Phuoc Loc. High-order axisymmetric Navier–Stokes code: Description and evaluation of boundary conditions. *International Journal for Numerical Methods in Fluids* 1987; **9**:1517.
33. Fix GJ, Rose ME. A comparative study of finite element and finite difference methods for Cauchy–Riemann type equations. *SIAM Journal of Numerical Analysis* 1985; **22**(2):250.
34. Gresho PM, Sani RL. On pressure boundary conditions for the incompressible Navier–Stokes equations. *International Journal for Numerical Methods in Fluids* 1987; **7**:1111.

